

# A Sinking Approach to Explore Arbitrary Areas in Free Energy Landscapes

Zhijun Pan<sup>1</sup>, Maodong Li<sup>1</sup>, Dechin Chen<sup>1</sup>, and Yi Isaac Yang<sup>1,\*</sup>

<sup>1</sup> Institute of Systems and Physical Biology, Shenzhen Bay Laboratory, Shenzhen 518132, China

\* To whom correspondence should be addressed: [yangyi@szbl.ac.cn](mailto:yangyi@szbl.ac.cn)

## Abstract

To address the time-scale limitations in molecular dynamics (MD) simulations, numerous enhanced sampling methods have been developed to expedite the exploration of complex free energy landscapes. A commonly employed approach accelerates the sampling of degrees of freedom associated with predefined collective variables (CVs), which typically tends to traverse the entire CV range. However, in many scenarios, the focus of interest is on specific regions within the CV space. In this paper, we introduce a novel “sinking” approach that enables enhanced sampling of arbitrary areas within the CV space. We begin by proposing a gridded convolutional approximation that productively replicates the effects of metadynamics, a powerful CV-based enhanced sampling technique. Building on this, we present the SinkMeta method, which “sinks” the interior bias potential to create a restraining potential “cliff” at the grid edges. This technique can confine the exploration of CVs in MD simulations to a predefined area. Our experimental results demonstrate that SinkMeta requires minimal sampling steps to estimate the free energy landscape for CV subspaces of various shapes and dimensions, including irregular two-dimensional regions and one-dimensional pathways between metastable states. We believe that SinkMeta will pioneer a new paradigm for sampling partial phase spaces, especially offering an efficient and flexible solution for sampling minimum free energy paths in high-dimensional spaces.

## Introduction

With the advancement of computing power and the widespread adoption of computational techniques, molecular modelling and simulation, exemplified by molecular dynamics (MD) and Monte Carlo (MC) simulations, have found extensive applications across various scientific disciplines. The essence of these atomistic and molecular simulations lies in sampling, which involves calculating the probability distributions of the physical properties or processes of interest within the simulation system. Specifically, computing the free energy surfaces (FES) corresponding to the collective variables (CVs) of interest is crucial for studying the system's thermodynamics. However, even with powerful supercomputers like Anton(1), the time scales currently achievable *in silico* often fall short of the requirements for computing complex FES.

As a result, enhanced sampling methods(2, 3) aimed at overcoming these time scale limitations have become an essential component of molecular modelling and simulations. Some enhanced sampling approaches facilitate the global acceleration of all degrees of freedom (DOFs) within the simulation system, such as replica-exchange molecular dynamics (REMD) (4, 5), simulated tempering(6), the Wang-Landau(7) algorithm, and integrated tempering sampling (ITS) (8, 9). These methods do not require prior setup of any CV and are relatively easy to use but typically offer limited acceleration for the physical processes in a specific partial phase space. Another class of enhanced sampling techniques is based on predefined CVs, such as umbrella sampling(10), local elevation(11), metadynamics (MetaD)(12) and variationally enhanced sampling (VES)(13). These methods accelerate only the DOFs associated with the CVs, generally resulting in higher sampling efficiency for specific physical properties.

MetaD(12) is a widely used enhanced sampling approach that explores the FES by introducing a history-dependent bias potential into the simulation system. The MetaD method has spawned several variants, with well-tempered metadynamics (WT-MetaD) (14) being the most significant improvement, addressing the convergence problem of the bias potential by adaptively adjusting the height of the Gaussian kernel accumulated at each step. WT-MetaD has become synonymous with MetaD. MetaD can also be combined with CV-free enhanced sampling methods, such as multiple walkers metadynamics (MW-MetaD) (15) and bias exchange metadynamics (BE-MetaD) (16, 17) in conjunction with REMD, and MetaITS(18, 19) in combination with ITS.

Despite the various new techniques, CV-based enhanced sampling methods like MetaD are still limited by the size of the CV space they can explore. The phase space that can be visited within a given number of simulation steps is finite, causing the required simulation time for sampling to grow almost exponentially with increasing CV dimensions. However, in many cases, it is unnecessary to search the entire CV space. When one needs to sample a specific region of the FES, additional restraining potentials must be introduced. Unfortunately, adding suitable restraining potentials to high-dimensional CV spaces to control the CV within a particular area is extremely challenging.

In this article, we propose a “sinking” approach adapted from MetaD that allows sampling the FES in arbitrary areas of the simulation system. We first introduce a gridded convolutional approximation that efficiently achieves the equivalent enhanced sampling effect as the MetaD method. Then, we construct a sinking bias potential based on this convolutional approach. This method automatically creates "cliffs" of restraining potentials at the edges of predefined CV grids, thus limiting the sampling of CVs to desired areas. Finally, we present examples of this approach for sampling specific regions with different shapes and dimensions in CV space and calculating their FES.

## Methodology

### A. Convolutional Metadynamics

Metadynamics (MetaD)(12) is an enhanced sampling method based on collective variables (CVs). CVs  $\mathbf{s}(\mathbf{R})$  is a set of functions of the atomic coordinates  $\mathbf{R}$  of the system, which can describe the physical behaviour of interest (20):  $\mathbf{s}(\mathbf{R}) = \{s_1(\mathbf{R}), s_2(\mathbf{R}), \dots, s_D(\mathbf{R})\}$ . The MetaD method achieves enhanced sampling by continuously accumulating Gaussian-type repulsive potentials  $\{G(\mathbf{s}(\mathbf{R}); t)\}$  in the space of CVs  $\mathbf{s}(\mathbf{R})$  into the bias potential  $V(\mathbf{s}; t)$ :

$$V(\mathbf{s}(\mathbf{R}); t) = \sum_t G(\mathbf{s}(\mathbf{R}); t) \tag{1}$$

$$G(\mathbf{s}(\mathbf{R}); t) = \omega(t) e^{-\frac{1}{2} \left\| \frac{\mathbf{s}(\mathbf{R}) - \mathbf{s}'(t)}{\sigma} \right\|^2} \tag{2}$$

where  $\mathbf{s}'(t)$  is the value of the CVs  $\mathbf{s}(\mathbf{R})$  at the simulation step  $t$ , and  $\omega(t)$  as well as  $\sigma$  is

the weight coefficient and standard deviation of the Gaussian function, respectively. The original MetaD method has a constant weight coefficient  $w$ , whereas the more popular well-tempered metadynamics (WT-MetaD)(14) uses a function  $\omega(t)$  that decreases gradually according to the previously accumulated bias potential  $V(\mathbf{s}; t - 1)$ :

$$\omega(t) = we^{-\left(\frac{1}{\gamma-1}\right)\beta V(\mathbf{s}'(t); t-1)} \quad (3)$$

where  $\beta = k_B T$ ,  $k_B$  is the Boltzmann constant and  $T$  is the simulation temperature,  $\gamma > 1$  is a bias factor constant. When  $\gamma \rightarrow +\infty$ ,  $\omega(t) = w$  is a constant value, i.e., equivalent to the original MetaD.

If using equation (1) to update the bias potential  $V(\mathbf{s}, t)$  in the program, the single-step computational consumption of MetaD will increase continuously with the growing number of Gaussian kernels  $\{G(\mathbf{s}(\mathbf{R}); t)\}$ . A common solution is to accumulate the sums of Gaussian kernels  $G(\mathbf{s}(\mathbf{R}); t)$  on  $N$  pre-defined CV-grids  $\{\mathbf{s}_i\}$ , (21) which is used by many software packages such as PLUMED(22) and COLVARS(23).

Here, we introduce a novel gridded convolutional approach. The convolution of two ‘‘small’’ Gaussian functions with standard deviation  $\sigma'$  is equal to a ‘‘large’’ Gaussian function with standard deviation  $\sigma = \sqrt{2}\sigma'$ :  $\int_{-\infty}^{+\infty} d\xi \exp\left\{-\frac{(\xi-\mu)^2}{2(\sigma')^2}\right\} \exp\left\{-\frac{(x-\xi)^2}{2(\sigma')^2}\right\} = \sigma' \sqrt{\pi} \exp\left\{-\frac{(x-\mu)^2}{2\sigma^2}\right\}$ . Therefore, we can construct a set of Gaussian-form basis functions with standard deviation  $\sigma' = \sigma/\sqrt{2}$  on the CV-grids  $\{\mathbf{s}_i\}$  to fit the Gaussian function  $G(\mathbf{s}(\mathbf{R}); t)$  with standard deviation  $\sigma$ :

$$\begin{aligned} G(\mathbf{s}(\mathbf{R}); t) &\approx \frac{\omega(t)}{C(t)} \sum_i^N \Delta S_i e^{-\frac{1}{2}\left\|\frac{\mathbf{s}_i - \mathbf{s}'(t)}{\sigma'}\right\|^2} e^{-\frac{1}{2}\left\|\frac{\mathbf{s}(\mathbf{R}) - \mathbf{s}_i}{\sigma'}\right\|^2} \\ &= \frac{\omega(t)}{C(t)} \sum_i^N \Delta S_i f_i(t) g_i(\mathbf{s}(\mathbf{R})) \end{aligned} \quad (4)$$

$$f_i(t) = e^{-\frac{1}{2}\left\|\frac{\mathbf{s}_i - \mathbf{s}'(t)}{\sigma'}\right\|^2} \quad (5)$$

$$g_i(\mathbf{s}(\mathbf{R})) = e^{-\frac{1}{2}\left\|\frac{\mathbf{s}(\mathbf{R}) - \mathbf{s}_i}{\sigma'}\right\|^2} \quad (6)$$

$$C(t) = \frac{1}{(\sqrt{2})^D} \sum_i \Delta S_i f_i(t) \approx \prod_d^D (\sigma'_d \sqrt{\pi}) \quad (7)$$

where  $\Delta S_i = \prod_d^D \Delta s_{i,d}$  is the product of each dimension of the  $i$ -th grid spacing  $\Delta \mathbf{s}_i = \{\Delta s_{i,1}, \Delta s_{i,2}, \dots, \Delta s_{i,D}\}$ ,  $g_i(\mathbf{s}(\mathbf{R}))$  is the  $i$ -th basis functions,  $f_i(t)$  is the weight coefficient of the basis function  $g_i(\mathbf{s})$ , and  $C(t)$  is the normalisation factor. To ensure an accurate fit, any grid spacing  $\Delta s_i$  should be less than half the standard deviation  $\sigma$ :  $\Delta s_i \leq 0.5\sigma$ . Figure 1a-c. show the schematic representations of the basis-functions  $\{g_i(\mathbf{s})\}$ , the weight coefficients  $\{f_i\}$  and the fitted Gaussian function  $G(\mathbf{s})$ , respectively. See Appendix-A for detailed information about the gridded approximation for Gaussian convolution.

Therefore, we can change equation (1) for calculating the bias potential  $V(\mathbf{s}(\mathbf{R}); t)$  as:

$$\begin{aligned} V(\mathbf{s}(\mathbf{R}); t) &= \sum_t G(\mathbf{s}(\mathbf{R}); t) \\ &\approx \sum_t \frac{\omega(t)}{C(t)} \sum_i^N \Delta S_i f_i(t) g_i(\mathbf{s}(\mathbf{R})) \\ &= \sum_i^N k_i(t) \Delta S_i e^{-\frac{1}{2} \left\| \frac{\mathbf{s}(\mathbf{R}) - \mathbf{s}_i}{\sigma'} \right\|^2} \\ &= \sum_i^N G_i(\mathbf{s}(\mathbf{R}); t) \end{aligned} \quad (8)$$

$$k_i(t) = \sum_t \frac{\omega(t)}{C(t)} f_i(t) \quad (9)$$

where  $G_i(\mathbf{s}(\mathbf{R}); t) = k_i(t) \Delta S_i \exp\{-\frac{1}{2} \left\| \frac{\mathbf{s}(\mathbf{R}) - \mathbf{s}_i}{\sigma'} \right\|^2\}$  is the Gaussian kernel at the  $i$ -th CV-grid (Figure 1c), and  $k_i(t)$  is the weight parameter of kernel  $G_i(\mathbf{s}(\mathbf{R}); t)$ . In this way, the updating of the bias potential  $V(\mathbf{s}, t)$  is performed by varying a fixed number of weight parameters  $\{k_i(t)\}$ , so the number of Gaussian kernels  $\{G_i(\mathbf{s}(\mathbf{R}); t)\}$  need to be calculated at each step  $t$  does not increase over the simulation time.

In practice, since the Gaussian is a local basis function, it is sufficient to fit the bias potential  $V(\mathbf{s})$  using only a few numbers of Gaussian kernels at the grids  $\{\mathbf{s}_i\}$  within a cutoff distance  $s_{\text{cut}}$  from the CV  $\mathbf{s}$ , rather than using all the kernels  $\{G_i(\mathbf{s}(\mathbf{R}); t)\}$ :

$$V(\mathbf{s}(\mathbf{R}); t) \approx \sum_i^{|\mathbf{s}(\mathbf{R}) - \mathbf{s}_i|_d \leq s_{\text{cut},d}} k_i(t) \Delta S_i e^{-\frac{1}{2} \left\| \frac{\mathbf{s}(\mathbf{R}) - \mathbf{s}_i}{\sigma'} \right\|^2} \quad (10)$$

where  $|\mathbf{s}(\mathbf{R}) - \mathbf{s}_i|_d \leq s_{\text{cut},d}$  means that the absolute value of the component of  $\mathbf{s}(\mathbf{R}) - \mathbf{s}_i$  in

each dimension  $d$  is less than or equal to  $s_{\text{cut}}$ . And when updating the weight parameters  $k_i(t)$  using equation (9), it is also acceptable to accumulate the weight coefficients  $f_i(t)$  only on the CV-grids  $\{s_i\}$  that are within the cutoff distance  $s_{\text{cut}}$ .

$$f_i(t) \approx \begin{cases} e^{-\frac{1}{2} \left\| \frac{s_i - s'(t)}{\sigma'} \right\|^2}, & |(s_i - s'(t))_d| \leq s_{\text{cut},d} \\ 0, & \text{otherwise} \end{cases} \quad (11)$$

The cutoff distance  $s_{\text{cut}}$  can be generally taken as  $s_{\text{cut}} \geq 2.5\sigma$ .

This convolutional metadynamics (ConvMeta) approach can fully reproduce the effects of enhanced sampling by the original or well-tempered MetaD, while also substantially decreases computational cost.

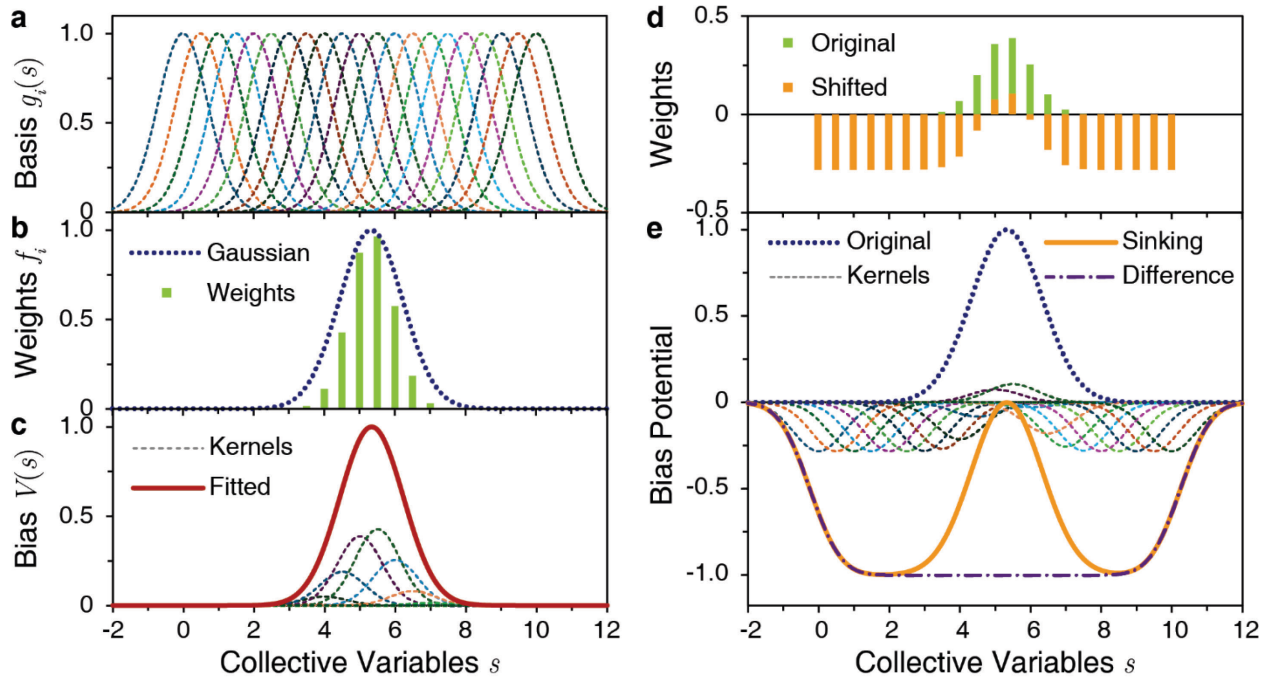


Figure 1. Schematic diagram of the bias potential of the ConvMeta and SinkMeta, where the sink depth  $E_{\text{depth}}$  of the bias maximum is 0. a) The Gaussian-type basis-functions  $\{g_i(s)\}$ . b) The weight coefficients  $\{f_i\}$  (green bar) of the basis functions used to fit a Gaussian function  $G(s)$  (blue dotted line). c) The fitted bias potential  $V(s)$  (red solid line) with the Gaussian kernels  $\{G_i(s)\}$  (coloured dashed line). d) The original (blue bars) and shifted (yellow bars) normalised weight coefficients of the basis functions. e) The bias potential of SinkMeta. The blue dotted line is the bias potential of the original MetaD, the yellow solid line is the bias potential of SinkMeta, the coloured dashed line is the Gaussian kernels and the violet dotted dashed line represents the

difference of bias potential between the sinking and original MetaD.

## B. “Sinking” Metadynamics

The bias potential  $V(\mathbf{s}(\mathbf{R}))$  of MetaD that consists of the kernels of repulsive Gaussian  $G(\mathbf{s}(\mathbf{R}))$  will drive the CV  $\mathbf{s}(\mathbf{R})$  away from the position it has already visited, thus forcing the sampling of the system to traverse the entire CV space. The size of the space to be explored increases exponentially with the dimension  $D$  of the CV  $\mathbf{s}(\mathbf{R})$ . Therefore, for adequate sampling with MetaD, the dimensionality of the CV  $\mathbf{s}(\mathbf{R})$  used must be very small, most commonly one or two, with three or above being relatively rare. Moreover, for non-periodic CV, the explorable space is theoretically infinite. Furthermore, it is also troublesome for the gridded approximation: once the CV  $\mathbf{s}(\mathbf{R})$  is squeezed out of the range of preset grids  $\{\mathbf{s}_i\}$ , the approach will fail. Thus, using non-periodic CVs in gridded MetaD usually requires building additional “walls” at the grid boundaries, i.e., restraining potentials for preventing CV from crossing the limit. However, the restraining potential of high-dimensional CVs is complicated to design.

Here, we propose a “sinking” approach adapted from the previously introduced ConvMeta approach, which uses the kernels of attractive potential to estimate the bias potential  $V(\mathbf{s}(\mathbf{R}))$ . If a shift factor  $v_{\text{shift}}(t)$  is subtracted for each of the weighting parameters  $\{k_i(t)\}$  in equation (8) (Figure 1d), then we will obtain a “sinking” bias potential  $V_{\text{sink}}(\mathbf{s}(\mathbf{R}); t)$ :

$$V_{\text{sink}}(\mathbf{s}(\mathbf{R}); t) = \sum_i^N [k_i(t) - v_{\text{shift}}(t)] \Delta S_i e^{-\frac{1}{2} \left\| \frac{\mathbf{s}(\mathbf{R}) - \mathbf{s}_i}{\sigma'} \right\|^2} = \sum_i^N G'_i(\mathbf{s}(\mathbf{R}); t) \quad (12)$$

where  $G'_i(\mathbf{s}(\mathbf{R}); t) = [k_i(t) - v_{\text{shift}}(t)] \Delta S_i \exp\{-\frac{1}{2} \left\| \frac{\mathbf{s}(\mathbf{R}) - \mathbf{s}_i}{\sigma'} \right\|^2\}$  is the “sinking” Gaussian kernel at the  $i$ -th CV-grid. When  $v_{\text{shift}}(t) > k_i(t)$ , the sinking Gaussian kernel  $G'_i(\mathbf{s}(\mathbf{R}); t)$  will turn from a repulsive potential to an attractive one. We hope the maximum value of the sinking bias potential  $V_{\text{sink}}(\mathbf{s}(\mathbf{R}); t)$  at any time  $t$  to be equal to a constant value  $-E_{\text{depth}}$  that is less than 0, where  $E_{\text{depth}}$  is the sinking depth of the bias potential maximum  $V_{\text{max}}(t)$ . Therefore, the shift factor  $v_{\text{shift}}(t)$  is:

$$v_{\text{shift}}(t) = \frac{V_{\text{max}}(t) + E_{\text{depth}}}{\prod_d^D(\sigma'_d \sqrt{2\pi})} = \frac{V_{\text{depth}}(t)}{C'} \quad (13)$$

$$V_{\text{depth}}(t) = V_{\text{max}}(t) + E_{\text{depth}} \quad (14)$$

where  $C' = \prod_d^D(\sigma'_d \sqrt{2\pi})$  is the normalisation constant,  $V_{\text{max}}(t)$  is the maximum value of the original bias potential  $V(\mathbf{s}(\mathbf{R}); t)$ , and  $V_{\text{depth}}(t)$  is the depth to which the interior region of the bias potential  $V(\mathbf{s}(\mathbf{R}), t)$ . See Appendix-B for detailed information about the shift factor.

We call this method SinkMeta. As shown in Figure 1e, most of the Gaussian kernels  $G'_i(\mathbf{s}(\mathbf{R}); t)$  become attractive potentials. As a result, the bias potential  $V_{\text{sink}}(\mathbf{s}(\mathbf{R}))$  in the interior region  $\mathcal{S}_{\text{inter}}$  of the CV grids  $\{\mathbf{s}_i\}$  “sank” by a constant value  $V_{\text{max}}$  compared to the original bias potential  $V(\mathbf{s}(\mathbf{R}))$ . This means that the system will be affected by the same bias force at this region as the original bias force  $\mathbf{F}(\mathbf{R}; t) = -\partial V(\mathbf{s}(\mathbf{R}))/\partial \mathbf{R}$  before “sinking”. While at the margins of the CV grids  $\{\mathbf{s}_i\}$ , the bias potential  $V_{\text{sink}}(\mathbf{s}(\mathbf{R}))$  form cliff-like restraining potentials, whose presence confines the sampling of the CV  $\mathbf{s}(\mathbf{R})$  in the interior of the grids  $\{\mathbf{s}_i\}$  and prevents it from crossing the boundary. See Appendix-C for detailed information about the boundary effect.

Therefore, SinkMeta can achieve the same sampling effect inside the CV grids as the ordinary WT-MetaD approach and, more importantly, without the risk of the CV escaping the grids after a long simulation time. It implies that we can set up irregular CV-grids in SinkMeta to achieve enhanced sampling of arbitrary regions of the free energy surface.

### C. Thermodynamics Calculation

The calculation of thermodynamic properties using SinkMeta is analogous to the WT-MetaD approach(14). When the update of the bias potential converges, the free energy  $F(\mathbf{s})$  corresponding to CV  $\mathbf{s}(\mathbf{R})$  at the interior region  $\mathcal{S}_{\text{inter}}$  of CV-grids  $\{\mathbf{s}_i\}$  can be calculated as:

$$F(\mathbf{s}) \propto -\left(\frac{\gamma}{\gamma - 1}\right) V_{\text{sink}}(\mathbf{s}), \quad (\mathbf{s} \in \mathcal{S}_{\text{inter}}) \quad (15)$$

Note that this formula cannot be used to compute the free energy of CVs outside the grids  $\{\mathbf{s}_i\}$ ,



and calculating CVs inside the grids but at the margins will also cause errors. Instead, the Boltzmann distribution  $p_0(\mathbf{R})$  of any observables in the system can be calculated as follows:

$$p_0(\mathbf{R}) = p(\mathbf{R})e^{\beta\{V_{\text{sink}}[\mathbf{s}(\mathbf{R});t]-c(t)\}} \quad (16)$$

$$\begin{aligned} c(t) &= \frac{1}{\beta} \log \frac{\int d\mathbf{s} e^{-\beta F(\mathbf{s})}}{\int d\mathbf{s} e^{-\beta[F(\mathbf{s})+V_{\text{sink}}(\mathbf{s};t)]}} \quad (17) \\ &\approx \frac{1}{\beta} \log \frac{\int d\mathbf{s} e^{-\frac{\gamma}{\gamma-1}\beta V(\mathbf{s};t)}}{\int d\mathbf{s} e^{-\frac{1}{\gamma-1}\beta V(\mathbf{s};t)}} - V_{\text{depth}}(t) \end{aligned}$$

where  $p(\mathbf{R})$  is the sampling probability obtained from MD simulations,  $c(t)$  is the revised factor(24, 25) for weights.

#### D. Code Available

We have implemented the ConvMeta and SinkMeta methods in the MD simulation software SPONGE(26) and MindSPONGE(27). The relevant code can be downloaded from the Gitee Code Repository: <https://gitee.com/d2denis/cudasponge-pan> (SPONGE) and <https://gitee.com/helloyesterday/mindsponge/tree/develop/> (MindSPONGE). The technical details and benchmark tests against well-established software can be found in the Supplementary Material.

## Results

### Sampling of the Complete CV space

First, we tested the ConvMeta and SinkMeta methods for sampling the entire CV space using a typical alanine dipeptide (ACE-ALA-NME) system in vacuum. We selected the Ramachandran dihedral angles  $\phi$  and  $\psi$  as the CVs, which are divided into 50\*50 uniform grids. The height  $w$  and standard deviation  $\sigma$  of the Gaussian-type potential are 2.0 kJ and 0.314 rad, respectively. The well-tempered bias factor  $\gamma$  for WT-MetaD is 10. We performed the MD simulations with ConvMeta and SinkMeta using a modified version of SPONGE. We also perform the MD simulation with conventional WT-MetaD having the same hyperparameters using the well-established software AMBER 24 with the PLUMED2.7 plug-in library.

Figure 2a-c shows the landscape of bias potentials obtained using ConvMeta and SinkMeta, WT-MetaD, respectively. It indicates that ConvMeta produces a bias potential identical to WT-MetaD's, demonstrating its consistency with the conventional MetaD approach. The landscape of bias potential generated by SinkMeta is also consistent with that of the traditional MetaD, except that its values are all negative. The free energy landscapes calculated using the three enhanced sampling methods are in perfect agreement (Figure 2d-f), all demonstrating the three metastable states  $C5$ ,  $C7_{eq}$  and  $C7_{ax}$  of the alanine dipeptide in vacuum. This indicates that SinkMeta can achieve the same sampling effect as the classical MetaD method for periodic CVs without boundaries.

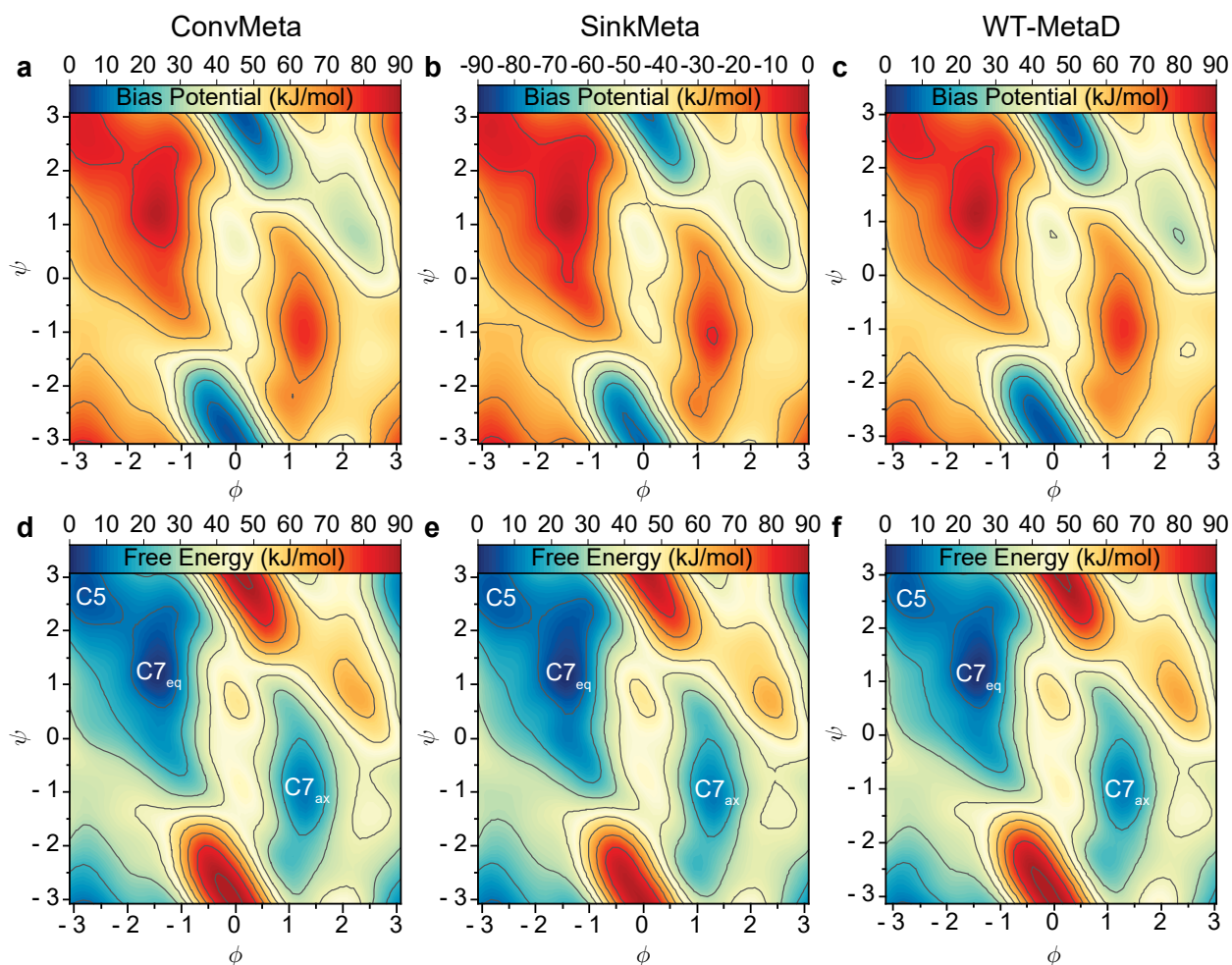


Figure 2. Landscape of the bias potential and free energy expressed as the function of the CVs  $(\phi, \psi)$ . a-c) The bias potential was obtained from ConvMeta, SinkMeta, and WT-MetaD, respectively. d-f) The free energy surface was calculated using conventional ConvMeta, SinkMeta, and WT-MetaD, respectively.

### Sampling for Specified CV Range

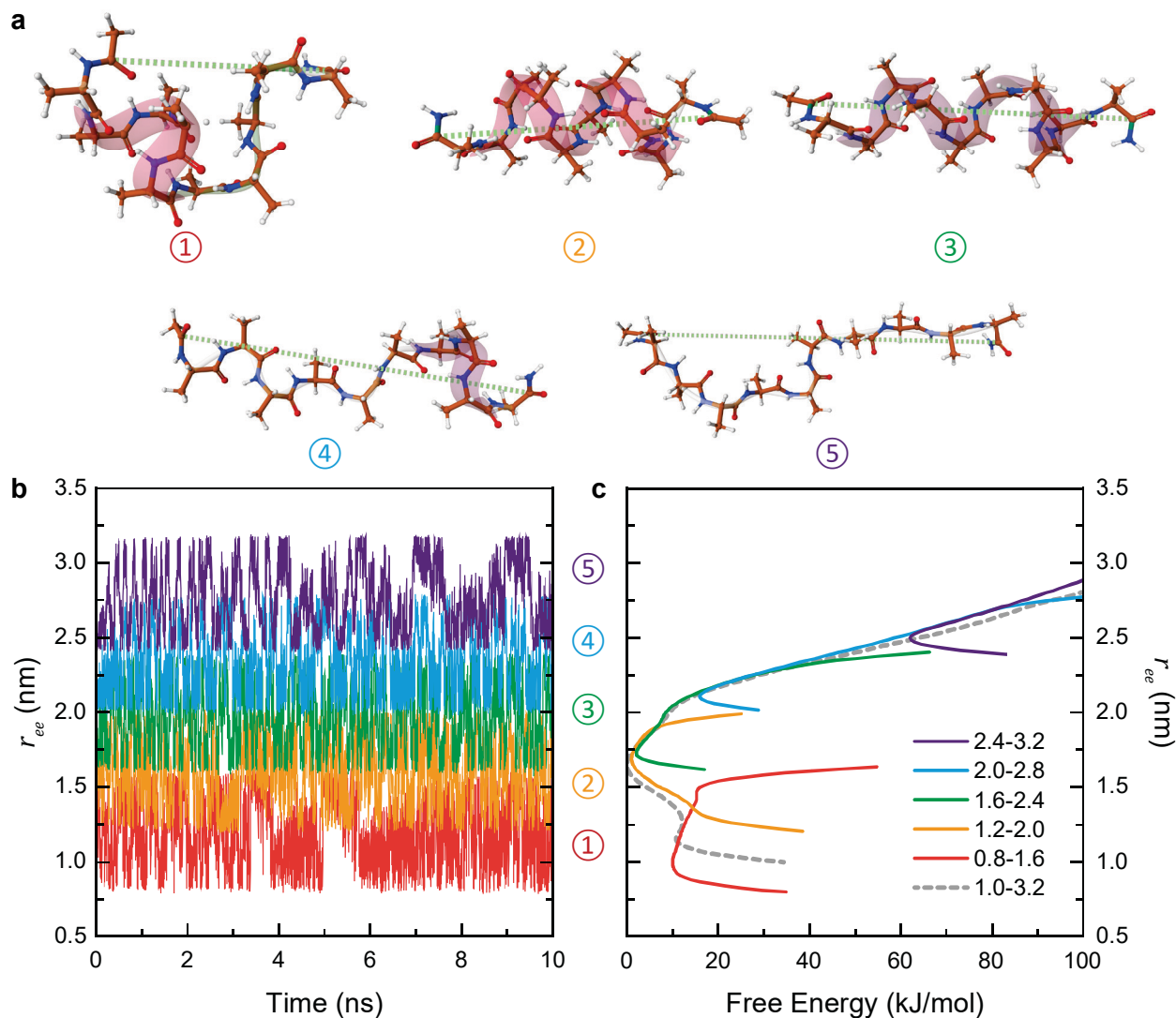


Figure 3. a) Conformations of deca-alanine at different end-to-end distances. b) Evolution of end-to-end distances in MD simulations with different CV ranges of SinkMeta. c) Free energy surface as a function of end-to-end distance calculated using different CV ranges of SinkMeta.

Then, we verified the sampling effect of SinkMeta for a specific CV range on the system of a capped decamer of alanine (hereafter referred to as deca-alanine) in vacuum. Deca-alanine has a noteworthy propensity to form  $\alpha$ -helix and, therefore has been a common system used in the theoretical investigation of conformational equilibria of short peptide segments.<sup>(28)</sup> Extension of deca-alanine can lead to its reversible unfolding, so a common way to study the system is to use its end-to-end distance  $r_{ee}$  as a CV for enhanced sampling in MD simulations. Distance is a non-

periodic CV with an infinite theoretical variable space (of course, there is a physical upper limit to the end-to-end distance of a peptide), and “pulling” the deca-alanine to different distances can make it change to different states (Figure 3a). Previously, if one wanted the system to transition between two specific neighbouring states, then pretty much the only way was to restrict the system, e.g. by adding upper and lower “walls” i.e. restraining potentials, at the sampling distances.

However, with SinkMeta, there is no need to go through this hassle. By simply setting a sampling range of values for the end-to-end distance  $r_{ee}$ , it is possible to keep the sampling of the system sampling only within that range of the CV in the MD simulation. Figure 3b shows the sampling effects of the MD simulation for the end-to-end distance  $r_{ee}$  of the system with different value ranges of CV were set in SinkMeta. The system will only strictly limit the sampling of CV  $r_{ee}$  to a pre-defined range of values without crossing the boundaries. Figure 3c shows the results of the free energy calculations for different preset ranges of CV. It implies that SinkMeta can estimate the free energy for a local phase space like umbrella sampling but with more convenience and flexibility in selecting the sampling space. See SI for more details.

### Sampling Irregular Area in CV Space

Next, we will demonstrate the sampling effectiveness of SinkMeta for arbitrary regions of CV space. Here, we still used the alanine dipeptide *in vacuo* as the testing system and utilised the dihedral angles  $(\phi, \psi)$  as CVs. This system has three meta-stable states C5, C7<sub>eq</sub> and C7<sub>ax</sub>, where C5 and C7<sub>eq</sub> are the two neighbouring states in phase space. If using conventional methods with such periodic CVs would sample the entire  $(\phi, \psi)$  space in the MD simulations, resulting in a free energy landscape like the one in Figure 2d-f. In contrast, using the SinkMeta method allows us just to sample a specific region of that space.

Here, we used SinkMeta to sample an irregular region where the alanine dipeptide's two metastable states C5 and C7<sub>eq</sub> are located. Conventional MetaD programs based on gridded approximations must spread the Gaussian kernel uniformly over the entire CV space. In contrast, with SinkMeta, we can preset the Gaussian basis function only in the regions around C5 and C7<sub>eq</sub>. Figure 4a illustrates the position of these Gaussian basis functions tiled in the  $(\phi, \psi)$  space.

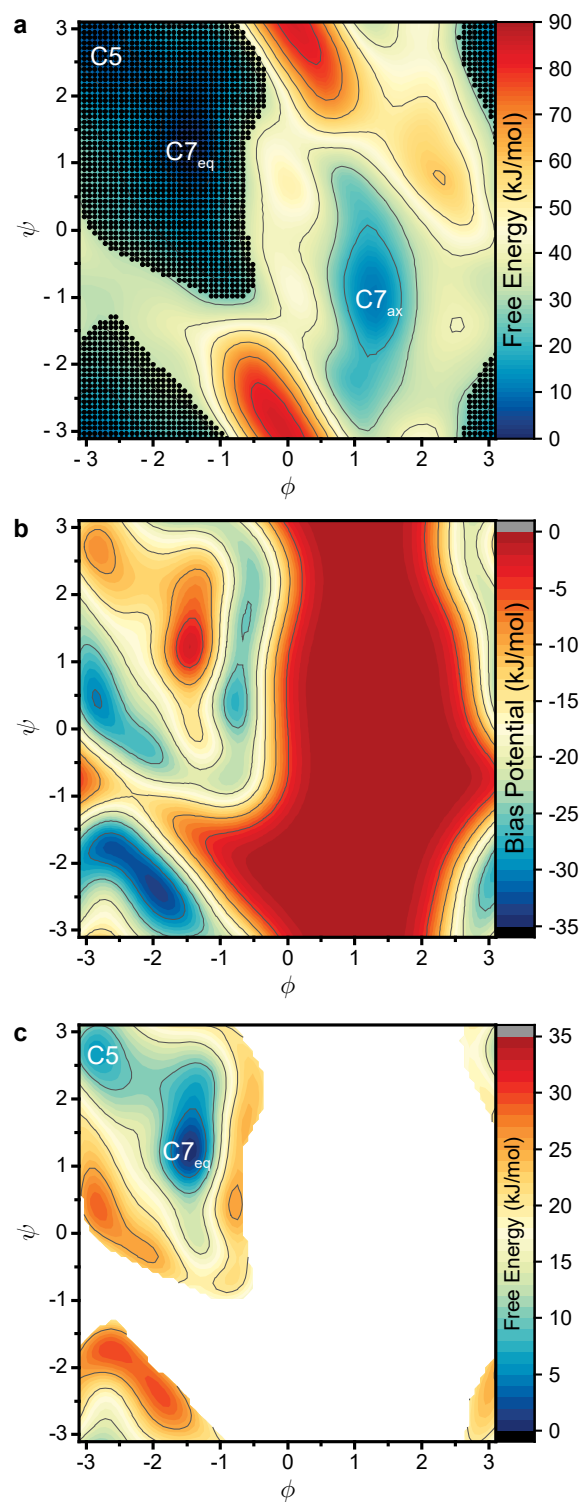


Figure 4. Enhanced sampling for regions where C5 and C7<sub>eq</sub> of alanine dipeptide are located. a) The position of Gaussian basis functions in the CV space. b) The bias potential generated by SinkMeta. c) Free energy surface as the function of  $(\phi, \psi)$  calculated using SinkMeta.

Using the SinkMeta method with these Gaussian basis functions as shown in Figure 4a, we can then make the sampling of the system confined to the region around  $C5$  and  $C7_{eq}$  states in the MD simulation. The bias potential obtained after the simulation is shown in Figure 4b. It displays that the bias potential is zero outside of the sampling region. The bias potentials within the sampling region are all negative, showing a ‘sinking’ state compared to other areas. This ‘sinking’ bias potential restrains the sampling of the system in the MD simulation to a pre-defined range of Gaussian grids, thus preventing it from escaping to other regions. Figure 4c shows the free surface calculated using the sampling results of the SinkMeta method after a 1 ns MD simulation. This suggests that SinkMeta has successfully reconstructed the local free energy landscape of the system in the vicinity of the  $C5$  and  $C7_{eq}$  states.

### Sampling Path in CV Space

The SinkMeta approach is very flexible in choosing a sampling area, which can be a subspace block with the same dimension in the CV space and even a direct reduction to a one-dimensional pathway. Here, we still used the alanine dipeptide system as an example to exhibit the enhanced sampling capability of SinkMeta on a specific path. Many path-searching methods have shown their ability to find the minimum free energy paths (MFEPs) of alanine dipeptide, such as nudged elastic band (NEB)(29-31), string methods(32-35) and traveling-salesman-based automated path searching (TAPS)(36). Typically, the paths were used for the post-analysis after MD simulations. The searched paths were sometimes used as reaction coordinates for umbrella sampling to estimate the free energy. Still, in many cases, it is not easy to define the paths as a few reaction coordinates that can be used as restraints.(30) However, SinkMeta does not have as many requirements for sampling a path in CV space as long as it is continuous and smooth.

Here, we used SinkMeta to sample a path between the  $C7_{eq}$  and  $C7_{ax}$  states of the alanine dipeptide. As shown in Figure 2d-f, the  $C7_{eq}$  and  $C7_{ax}$  states are the two dominant metastable states of the system, for which a high energy barrier features between them. We searched for a MFEP from  $C7_{eq}$  to  $C7_{ax}$  on the free energy landscape of the system in  $(\phi, \psi)$  space using NEB. Then, we placed a series of Gaussian basis functions along this path (Figure 5a). To avoid errors at the margins of the path, we extended both ends of the path to locations with high free energy, resulting in a total of 92 basis functions being arranged.

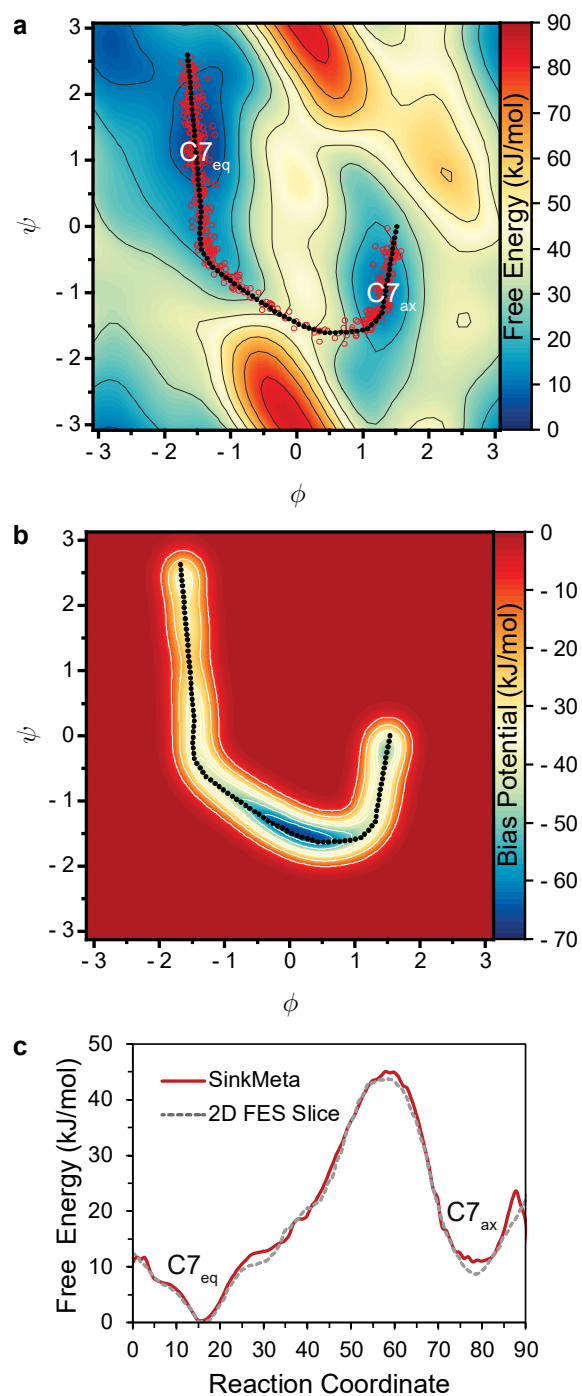


Figure 5. Sampling of the path between  $C7_{eq}$  and  $C7_{ax}$  states of the alanine dipeptide in vacuum using SinkMeta. a) Free energy surface as a function of dihedral angles  $\phi$  and  $\psi$ . The black dots are the location of Gaussian basis functions, and the red circles are the footprint left by the evolution of CV during MD simulation. b) The bias potential in the  $(\phi, \psi)$  space. c) Free energy surfaces with paths as reaction coordinates. The red solid line is the free energy calculated using the SinkMeta method with the path as the sampling region, while the grey dashed line is the

sliced value of the 2D free energy surface over the path.

Using SinkMeta can achieve highly efficient path sampling. As shown in Figure 5a, the evolution of the CVs was always concentrated near the path during the MD simulation. This is because the sinking bias potential produced by the SinkMeta “attracted” the CVs to the path (Figure 5b). This allows us to quickly transition between  $C7_{eq}$  to  $C7_{ax}$  states in a very short simulation time. After 1 ns of MD simulation, we can calculate the system's FES with the path as the reaction coordinate (Figure 5c). This free energy calculated using SinkMeta is in identical agreement with the result of slicing from the 2D FES free energy surface.

## Discussion and Conclusion

This paper introduces two novel enhanced sampling approaches, ConvMeta and SinkMeta, evolving from the MetaD method. ConvMeta employs a gridded convolutional approximation to fit the Gaussian kernel, achieving an equivalent enhanced sampling effect as MetaD, but more efficiently. Building on ConvMeta, SinkMeta transforms the repulsive Gaussian kernel into an attractive one, creating a “sinking” bias potential with restraining potential at the edges. This effectively limits the exploration of the CVs to the desired region, significantly reducing the required simulation time for sampling. We validated the sampling effectiveness of SinkMeta using the alanine dipeptide and deca-alanine systems, covering complete CV spaces, specific CV ranges, irregular CV areas, and one-dimensional paths in high-dimensional CV spaces. Our experimental results indicate that SinkMeta can flexibly achieve efficient enhanced sampling of arbitrary CV regions.

Technically, SinkMeta can sample a specific CV space using a custom grid or a uniform grid with a mask. Our gridded convolutional approach replicates the bias potential and can be viewed as a particular case of Gaussian-mixture-based methods(37-39), where each basis function shares the same hyperparameters. Thus, with a uniform grid, the cut-off distance can be quickly calculated (Equation (9) and (10)). While a custom grid offers more flexibility, it complicates the cut-off distance calculation. Users can choose the appropriate grid form based on their needs. Generally, if the mask space occupies a large proportion of the CV space, uniform grids with the mask are suitable. Conversely, custom grids are preferable when the grid dimension is smaller than the CV



dimension (e.g., a one-dimensional path in a high-dimensional CV space).

Using ConvMeta and SinkMeta to sample incomplete CV space requires attention to grid edge effects. Equation (4) calculates the Gaussian kernel based on infinite integral, but this integration condition is unmet at grid margins. Additionally, SinkMeta produces a “wall” of restraining potentials at grid edges, which also causes bias potential errors. Therefore, the grid should include some redundancy by expanding the sampling area by at least  $2\sigma$ . Moreover, avoid placing outermost grids with prominent shapes (e.g., the two terminals of a one-dimensional path in high-dimensional CV space) in the free energy basin to prevent excessive bias potential accumulation.

When using SinkMeta for MD simulations, the system's starting structure should be within the grids. SinkMeta generates restraining potentials only at grid margins, with zero bias potentials far from the grids. Thus, the initial CV in the simulation should not be outside the grids. Additionally, it will be difficult to return if the CV escapes the grid area during the simulation. This drawback can be mitigated by increasing the sinking depth  $E_{\text{depth}}$ . We are also developing a new restraining potential to address this issue.

We believe that this “sinking” approach opens a new paradigm for enhanced sampling. Traditionally, CV-free enhanced sampling methods accelerate all DOFs of the system, while CV-based methods accelerate only the CV-related DOFs. However, even CV-based methods typically sample the entire CV space, which is unnecessary for many scenarios. Sampling local CV space generally requires setting up complex restraining potentials, but it is often challenging. In contrast, SinkMeta does not require additional restraining potentials to sample any region in the CV space.

As a special case, SinkMeta is highly suitable for path sampling. Previous works have typically used umbrella sampling(40-42) or Path-CV(43, 44) for path sampling. Compared to umbrella sampling(10), SinkMeta allows a continuous transition of CVs along the entire path. While Path-CV(45, 46) transforms the points on the path into two CVs (i.e., the progress  $s$  along the path and the distance  $z$  from the path) and performs enhanced sampling on these 2D CVs  $(s, z)$ . SinkMeta directly explores the CVs along the one-dimensional path in the original CV space. Given the small CV space to be sampled, SinkMeta requires only a short simulation time to estimate the free energy landscape along the path accurately. Therefore, SinkMeta is an efficient and flexible method for path sampling.

The SinkMeta method also has the potential to be combined with path-searching methods and artificial intelligence (AI). The flexible grid settings in SinkMeta make it possible to achieve more efficient sampling by integrating path-searching methods. Additionally, recent advances in AI(27, 47) in molecular modelling and simulations have provided significant insights, especially deep reinforcement learning(48), which is well-suited for optimising enhanced sampling parameters(49). If reinforcement learning can dynamically adjust SinkMeta grids during MD simulations, it is possible to realise intelligent simulation and sampling.

## **Acknowledgement**

The authors thank Yi Qin Gao, Xu Han, Yijie Xia, Haohao Fu and Lizhe Zhu for useful discussion. Computational resources were supported by Shenzhen Bay Laboratory supercomputing centre. This work was supported by the National Science and Technology Major Project (No. 2022ZD0115003) and the National Natural Science Foundation of China (22273061 to Y.I.Y).

## Appendix

### A. Gridded Approximation for Gaussian Convolution

We set the convolution of Gaussian functions  $f(x) = g(x) = e^{-\frac{x^2}{2(\sigma')^2}}$  as  $\mathcal{G}(x)$ :

$$\mathcal{G}(x) = (f * g)(x) = \int_{-\infty}^{+\infty} d\tau f(\tau)g(x - \tau) \quad (\text{S1})$$

Thus, the function  $\mathcal{G}(x - \mu)$  is:

$$\mathcal{G}(x - \mu) = (f * g)(x - \mu) = \int_{-\infty}^{+\infty} d\tau f(\tau)g(x - \mu - \tau) \quad (\text{S2})$$

Set  $\xi = \tau + \mu$ , then:

$$\begin{aligned} \mathcal{G}(x - \mu) &= \int_{-\infty}^{+\infty} d\xi f(\xi - \mu)g(x - \xi) \\ &= \int_{-\infty}^{+\infty} d\xi e^{-\frac{(\xi - \mu)^2}{2(\sigma')^2}} e^{-\frac{(x - \xi)^2}{2(\sigma')^2}} \\ &= \int_{-\infty}^{+\infty} d\xi e^{-\frac{x^2 + \mu^2 - 2(x + \mu)\xi + 2\xi^2}{2(\sigma')^2}} \\ &= \int_{-\infty}^{+\infty} d\xi e^{-\frac{(x - \mu)^2}{2(\sigma')^2}} e^{-\frac{(x + \mu)^2 - 2(x + \mu)\xi + 2\xi^2}{2(\sigma')^2}} \\ &= e^{-\frac{(x - \mu)^2}{2(\sqrt{2}\sigma')^2}} \int_{-\infty}^{+\infty} d\xi e^{-\frac{(x + \mu - \xi)^2}{(\sigma')^2}} \\ &= \sigma' \sqrt{\pi} e^{-\frac{(x - \mu)^2}{2\sigma^2}} \end{aligned} \quad (\text{S3})$$

where  $\sigma = \sqrt{2}\sigma'$ . It indicates that a “large” Gaussian function  $\exp\left\{-\frac{(x - \mu)^2}{2\sigma^2}\right\}$  with a standard deviation of  $\sigma$  can be represented by a convolution of two “small” Gaussian functions  $\exp\left\{-\frac{(\xi - \mu)^2}{2(\sigma')^2}\right\}$  and  $\exp\left\{-\frac{(x - \xi)^2}{2(\sigma')^2}\right\}$  with a standard deviation of  $\sigma' = \sigma/\sqrt{2}$ :

$$e^{-\frac{(x - \mu)^2}{2\sigma^2}} = \frac{1}{\sigma' \sqrt{\pi}} \int_{-\infty}^{+\infty} d\xi e^{-\frac{(\xi - \mu)^2}{2(\sigma')^2}} e^{-\frac{(x - \xi)^2}{2(\sigma')^2}} \quad (\text{S4})$$

And a  $D$ -dimensional multivariate Gaussian function  $G(\mathbf{x} - \boldsymbol{\mu})$  can be expressed as:

$$\begin{aligned}
G(\mathbf{x} - \boldsymbol{\mu}) &= e^{-\frac{1}{2}(\mathbf{x}-\boldsymbol{\mu})^T \boldsymbol{\Sigma}^{-1}(\mathbf{x}-\boldsymbol{\mu})} \\
&= \frac{1}{C} \int_{-\infty}^{+\infty} d\xi f(\xi - \boldsymbol{\mu}) g(\mathbf{x} - \xi) \\
&= \frac{1}{C} \int_{-\infty}^{+\infty} d\xi e^{-(\xi-\boldsymbol{\mu})^T \boldsymbol{\Sigma}^{-1}(\xi-\boldsymbol{\mu})} e^{-(\mathbf{x}-\xi)^T \boldsymbol{\Sigma}^{-1}(\mathbf{x}-\xi)}
\end{aligned} \tag{S5}$$

$$C = \sqrt{\pi^D \det(\boldsymbol{\Sigma})} \tag{S6}$$

where  $C$  is the normalisation factor,  $\boldsymbol{\Sigma}$  is the covariance matrix of the multivariate Gaussian function  $\mathcal{G}(\mathbf{x} - \boldsymbol{\mu})$ ,  $\boldsymbol{\Sigma}^{-1}$  is its inverse, and  $\det(\boldsymbol{\Sigma})$  denotes the determinant of  $\boldsymbol{\Sigma}$ . But in most cases, we will only use the diagonal matrix as the covariance matrix, that is, use a  $D$ -dimensional vector as the standard deviation  $\boldsymbol{\sigma} = \{\sigma_1, \sigma_2, \dots, \sigma_D\}$ :

$$G(\mathbf{x} - \boldsymbol{\mu}) = e^{-\frac{1}{2}\|\frac{\mathbf{x}-\boldsymbol{\mu}}{\boldsymbol{\sigma}}\|^2} = \frac{1}{C} \int_{-\infty}^{+\infty} d\xi e^{-\frac{1}{2}\|\frac{\xi-\boldsymbol{\mu}}{\boldsymbol{\sigma}'}\|^2} e^{-\frac{1}{2}\|\frac{\mathbf{x}-\xi}{\boldsymbol{\sigma}'}\|^2} \tag{S7}$$

$$C = \sqrt{\pi^D \det(\text{diag}(\boldsymbol{\sigma}))} = \prod_d (\sigma_d \sqrt{\pi}) = \prod_d \left( \sigma_d \sqrt{\frac{\pi}{2}} \right) \tag{S8}$$

Therefore, we can fit the Gaussian-type repulsive potential  $G[\mathbf{s}(\mathbf{R}); \mathbf{s}'(t)]$  of MetaD with a set of Gaussian-type basis-functions  $g_i(\mathbf{s}) = \exp(-\frac{1}{2}\|\frac{\mathbf{s}-\mathbf{s}_i}{\boldsymbol{\sigma}'}\|^2)$  at the CV-grids  $\{\mathbf{s}_i\}$  with spacing  $\{\Delta S_i = \prod_d \Delta s_{i,d}\}$ :

$$G[\mathbf{s}(\mathbf{R}); \mathbf{s}'(t)] = \omega(t) e^{-\frac{1}{2}\|\frac{\mathbf{s}(\mathbf{R})-\mathbf{s}'(t)}{\boldsymbol{\sigma}}\|^2} = \frac{\omega(t)}{C(t)} \sum_i \Delta S_i f_i(\mathbf{s}'(t)) g_i(\mathbf{s}(\mathbf{R})) \tag{S9}$$

$$f_i(\mathbf{s}'(t)) = e^{-\frac{1}{2}\|\frac{\mathbf{s}_i-\mathbf{s}'(t)}{\boldsymbol{\sigma}'}\|^2} = e^{-\|\frac{\mathbf{s}_i-\mathbf{s}'(t)}{\boldsymbol{\sigma}'}\|^2} \tag{S10}$$

$f_i(\mathbf{s}'(t))$  is the weight coefficient of basis  $g_i(\mathbf{s}(\mathbf{R}))$ . We expect the integral of the fitted function to be equal to the integral of the original function, i.e.:

$$\begin{aligned}
\int_{-\infty}^{+\infty} d\mathbf{s} e^{-\frac{1}{2}\|\frac{\mathbf{s}-\mathbf{s}'(t)}{\boldsymbol{\sigma}}\|^2} &= \int_{-\infty}^{+\infty} d\mathbf{s} \frac{1}{C(t)} \sum_i \Delta S_i f_i(t) e^{-\frac{1}{2}\|\frac{\mathbf{s}-\mathbf{s}_i}{\boldsymbol{\sigma}'}\|^2} \\
\prod_d (\sigma_d \sqrt{2\pi}) &= \frac{1}{C(t)} \prod_d (\sigma_d \sqrt{\pi}) \sum_i \Delta S_i f_i(t)
\end{aligned} \tag{S11}$$

Thus, the normalisation factor  $C(t)$  is:

$$C(t) = \frac{1}{(\sqrt{2})^D} \sum_i \Delta S_i f_i(t) \quad (\text{S12})$$

If  $\mathbf{s}'(t)$  is not located at the margins of CV-grids  $\{\mathbf{s}_i\}$ , then according to equation (S7), there is:

$$C(t) = \frac{1}{(\sqrt{2})^D} \sum_i \Delta S_i f_i(t) \approx C = \prod_d (\sigma'_d \sqrt{\pi}) \quad (\text{S13})$$

Thus, the normalisation factor  $C(t)$  can also be approximated as a constant  $C$ :

## B. Shift Factor

We obtain the sinking bias potential  $V_{\text{sink}}(\mathbf{s}(\mathbf{R}); t)$  by subtracting a shift factor  $v_{\text{shift}}(t)$  from each weighting parameter  $k_i(t)$ :

$$\begin{aligned} V_{\text{sink}}(\mathbf{s}(\mathbf{R}); t) &= \sum_i^N (k_i(t) - v_{\text{shift}}(t)) \Delta S_i e^{-\frac{1}{2} \left\| \frac{\mathbf{s}(\mathbf{R}) - \mathbf{s}_i}{\sigma'} \right\|^2} \\ &= \sum_i^N k_i(t) \Delta S_i e^{-\frac{1}{2} \left\| \frac{\mathbf{s}(\mathbf{R}) - \mathbf{s}_i}{\sigma'} \right\|^2} - v_{\text{shift}}(t) \sum_i^N \Delta S_i e^{-\frac{1}{2} \left\| \frac{\mathbf{s}(\mathbf{R}) - \mathbf{s}_i}{\sigma'} \right\|^2} \\ &= V(\mathbf{s}(\mathbf{R}), t) - v_{\text{shift}}(t) \Phi(\mathbf{s}(\mathbf{R})) \\ &= V(\mathbf{s}(\mathbf{R}), t) + V_{\text{shift}}(\mathbf{s}(\mathbf{R}); t) \end{aligned} \quad (\text{S14})$$

$$\Phi(\mathbf{s}) = \sum_i^N \Delta S_i e^{-\frac{1}{2} \left\| \frac{\mathbf{s}(\mathbf{R}) - \mathbf{s}_i}{\sigma'} \right\|^2} \quad (\text{S15})$$

where  $\Phi(\mathbf{s})$  is the cumulative function, and  $V_{\text{shift}}(\mathbf{s}(\mathbf{R}); t) = -v_{\text{shift}}(t) \Phi(\mathbf{s}(\mathbf{R}))$  is the shift potential. We expect the maximum value of the sinking bias potential  $V_{\text{sink}}(\mathbf{s}(\mathbf{R}), t)$  to be a manually constant value  $-E_{\text{depth}}$ :

$$\begin{aligned} \max\{V_{\text{sink}}(\mathbf{s}; t)\} &= \max\{V(\mathbf{s}; t) - v_{\text{shift}}(t) \Phi(\mathbf{s})\} \\ &= V_{\text{max}}(t) - v_{\text{shift}}(t) \Phi[\mathbf{s}(V_{\text{max}}(t))] \\ &= -E_{\text{depth}} \end{aligned} \quad (\text{S16})$$

where  $V_{\text{max}}(t)$  is the maximum value of the original bias potential  $V(\mathbf{s}; t)$ , and  $\mathbf{s}(V_{\text{max}}(t))$  is the CV corresponding to  $V_{\text{max}}(t)$ . Consider that the bias potential maximum  $V_{\text{max}}(t)$  is generally not located at the margins of the CV-grids  $\{\mathbf{s}_i\}$ , so  $\Phi[\mathbf{s}(V_{\text{max}}(t))]$  can be estimated as:

$$\Phi[\mathbf{s}(V_{\text{max}}(t))] = \sum_i^N \Delta S_i e^{-\frac{1}{2} \left\| \frac{\mathbf{s}(V_{\text{max}}(t)) - \mathbf{s}_i}{\sigma'} \right\|^2} \approx \prod_d (\sigma'_d \sqrt{2\pi}) = C' \quad (\text{S17})$$

where  $C' = \prod_d^D (\sqrt{2\pi} \sigma'_d) = (\sqrt{2})^D C$  is a constant. Therefore, the shift factor  $v_{\text{shift}}(t)$  is:

$$v_{\text{shift}}(t) = \frac{V_{\text{max}}(t) + E_{\text{depth}}}{\Phi[\mathbf{s}(V_{\text{max}}(t))]} \approx \frac{V_{\text{depth}}(t)}{\prod_d^D(\sigma'_d \sqrt{2\pi})} = \frac{V_{\text{depth}}(t)}{(\sqrt{2})^D C} \quad (\text{S18})$$

where  $V_{\text{depth}}(t) = V_{\text{max}}(t) + E_{\text{depth}}$  is the depth to which the interior region of the bias potential  $V(\mathbf{s}(\mathbf{R}), t)$ .

### C. Boundary Effect

The bias force  $\mathbf{F}_{\text{sink}}(\mathbf{R}; t)$  of SinkMeta is:

$$\begin{aligned} \mathbf{F}_{\text{sink}}(\mathbf{R}; t) &= -\frac{\partial V_{\text{sink}}(\mathbf{s}(\mathbf{R}); t)}{\partial \mathbf{R}} \\ &= -\frac{\partial V(\mathbf{s}(\mathbf{R}); t)}{\partial \mathbf{R}} - \frac{\partial V_{\text{shift}}(\mathbf{s}(\mathbf{R}); t)}{\partial \mathbf{R}} \\ &= \mathbf{F}(\mathbf{R}; t) + \mathbf{F}_{\text{shift}}(\mathbf{R}; t) \end{aligned} \quad (\text{S19})$$

where  $\mathbf{F}(\mathbf{R}; t) = -\partial V(\mathbf{s}(\mathbf{R}; t))/\partial \mathbf{R}$  is the original bias force before sinking,  $\mathbf{F}_{\text{shift}}(\mathbf{R}; t) = v_{\text{shift}}(t) \partial (\Phi(\mathbf{s}(\mathbf{R}))) / \partial \mathbf{R}$  is the shift force. Here, we use  $\mathbf{S}$  to denote the space where the CV-grids  $\{s_i\}$  is located, then the cumulative function  $\Phi(\mathbf{s}(\mathbf{R}))$  can be expressed as follow:

$$\Phi(\mathbf{s}) = \sum_i^N \Delta S_i e^{-\frac{1}{2} \left\| \frac{\mathbf{s} - \mathbf{s}_i}{\sigma'} \right\|^2} \approx \int_{\mathbf{S}} d\xi e^{-\frac{1}{2} \left\| \frac{\xi - \mathbf{s}}{\sigma'} \right\|^2} \quad (\text{S20})$$

Let us first consider the case of one-dimensional CV  $s$ . In this situation,  $\Phi(s)$  can be approximated as the integral from the lower bound  $s_{\text{min}}$  to the upper bound  $s_{\text{max}}$  of the CV grids  $\{s_i\}$ :

$$\begin{aligned} \Phi(s) &\approx \int_{s_{\text{min}}}^{s_{\text{max}}} d\xi e^{-\frac{1}{2} \left( \frac{\xi - s}{\sigma'} \right)^2} \\ &= \frac{\sigma' \sqrt{2\pi}}{2} \left[ \text{erf} \left( \frac{s_{\text{max}} - s}{\sigma' \sqrt{2}} \right) - \text{erf} \left( \frac{s_{\text{min}} - s}{\sigma' \sqrt{2}} \right) \right] \end{aligned} \quad (\text{S21})$$

Then, the shift potential  $V_{\text{shift}}(s; t)$  is:

$$\begin{aligned} V_{\text{shift}}(s; t) &= -v_{\text{shift}}(t) \Phi(s) \\ &\approx \frac{1}{2} V_{\text{depth}}(t) \left[ \text{erf} \left( \frac{s - s_{\text{max}}}{\sigma' \sqrt{2}} \right) - \text{erf} \left( \frac{s - s_{\text{min}}}{\sigma' \sqrt{2}} \right) \right] \end{aligned} \quad (\text{S22})$$

As a result, the shift potential  $V_{\text{shift}}(s, t)$  is equivalent to forming ‘‘cliffs’’ at the margins of

the CV grids  $\{s_i\}$  with the lower and upper restraining potentials  $V_{\text{rest}}^{\text{lower}}(s; t)$  and  $V_{\text{rest}}^{\text{upper}}(s; t)$ :

$$V_{\text{rest}}^{\text{lower}}(s; t) = -\frac{1}{2}V_{\text{depth}}(t) \left[ 1 + \operatorname{erf} \left( \frac{s - s_{\text{min}}}{\sigma' \sqrt{2}} \right) \right] \quad (\text{S23})$$

$$V_{\text{rest}}^{\text{upper}}(s; t) = -\frac{1}{2}V_{\text{depth}}(t) \left[ 1 - \operatorname{erf} \left( \frac{s - s_{\text{max}}}{\sigma' \sqrt{2}} \right) \right] \quad (\text{S24})$$

And the lower and upper restraining forces  $F_{\text{rest}}^{\text{lower}}(s; t)$  and  $F_{\text{rest}}^{\text{upper}}(s; t)$  are:

$$F_{\text{rest}}^{\text{lower}}(s; t) = -\frac{\partial(V_{\text{rest}}^{\text{lower}}(s; t))}{\partial s} = \frac{V_{\text{depth}}(t)}{\sigma' \sqrt{2\pi}} e^{-\frac{1}{2}\left(\frac{s-s_{\text{min}}}{\sigma'}\right)^2} \quad (\text{S25})$$

$$F_{\text{restr}}^{\text{upper}}(s; t) = -\frac{\partial(V_{\text{rest}}^{\text{upper}}(s; t))}{\partial s} = -\frac{V_{\text{depth}}(t)}{\sigma' \sqrt{2\pi}} e^{-\frac{1}{2}\left(\frac{s-s_{\text{max}}}{\sigma'}\right)^2} \quad (\text{S26})$$

The upper and lower restraining potentials  $V_{\text{rest}}^{\text{lower}}(s; t)$  and  $V_{\text{rest}}^{\text{upper}}(s; t)$  will confine the CV  $s$  to the interior of the grids  $\{s_i\}$ .

And the shift bias  $V_{\text{shift}}^{\text{inter}}(s; t)$  at the grid interior equal to a constant value  $-V_{\text{depth}}(t)$ , so the bias force  $F_{\text{sink}}^{\text{inter}}(\mathbf{R}; t)$  of SinkMeta at this region is approximated to the original bias force  $F(\mathbf{R}; t)$  before sinking:

$$F_{\text{sink}}^{\text{inter}}(\mathbf{R}; t) = F(\mathbf{R}; t) - \frac{\partial V_{\text{shift}}^{\text{inter}}(s; t)}{\partial \mathbf{R}} \approx F(\mathbf{R}; t) \quad (\text{S27})$$

The case of multidimensional CV  $s(\mathbf{R})$  is analogous to that of one-dimensional. The restraining potential  $V_{\text{shift}}^{\text{margin}}(s(\mathbf{R}))$  at the margins of the CV-grids  $\{s_i\}$  will prevent CVs  $s(\mathbf{R})$  from escaping to the exterior of the grids  $\{s_i\}$ , while CVs trapped in the grid interior will be under the same bias force  $F(\mathbf{R}; t)$  as in the regular WT-MetaD approach.

## Reference

1. D. E. Shaw, M. M. Deneroff, R. O. Dror, J. S. Kuskin, R. H. Larson *et al.*, Anton, a special-purpose machine for molecular dynamics simulation. *Commun. ACM* **51**, 91-97 (2008).
2. Y. I. Yang, Q. Shao, J. Zhang, L. Yang, Y. Q. Gao, Enhanced sampling in molecular dynamics. *J. Chem. Phys.* **151**, 070902 (2019).
3. J. Hénin, T. Lelièvre, M. R. Shirts, O. Valsson, L. Delemotte, Enhanced Sampling Methods for Molecular Dynamics Simulations [Article v1.0]. *Living J. Comput. Mol. Sci.* **4**, 1583

- (2022).
4. R. H. Swendsen, J.-S. Wang, Replica Monte Carlo Simulation of Spin-Glasses. *Phys. Rev. Lett.* **57**, 2607-2609 (1986).
  5. Y. Sugita, Y. Okamoto, Replica-exchange molecular dynamics method for protein folding. *Chem. Phys. Lett.* **314**, 141-151 (1999).
  6. E. Marinari, G. Parisi, Simulated Tempering: A New Monte Carlo Scheme. *Europhys. Lett.* **19**, 451 (1992).
  7. F. Wang, D. P. Landau, Efficient, Multiple-Range Random Walk Algorithm to Calculate the Density of States. *Phys. Rev. Lett.* **86**, 2050-2053 (2001).
  8. Y. Q. Gao, An integrate-over-temperature approach for enhanced sampling. *J. Chem. Phys.* **128**, 064105 (2008).
  9. X. Han, Y.-K. Lei, M. Li, Y. Q. Gao, A brief review of integrated tempering sampling molecular simulation. *Chem. Phys. Rev.* **5** (2024).
  10. G. M. Torrie, J. P. Valleau, Nonphysical sampling distributions in Monte Carlo free-energy estimation: Umbrella sampling. *J. Comput. Phys.* **23**, 187-199 (1977).
  11. T. Huber, A. E. Torda, W. F. van Gunsteren, Local elevation: A method for improving the searching properties of molecular dynamics simulation. *J. Comput. Aided Mol. Des.* **8**, 695-708 (1994).
  12. A. Laio, M. Parrinello, Escaping free-energy minima. *Proc. Nat. Acad. Sci. U.S.A.* **99**, 12562-12566 (2002).
  13. O. Valsson, M. Parrinello, Variational Approach to Enhanced Sampling and Free Energy Calculations. *Phys. Rev. Lett.* **113**, 090601 (2014).
  14. A. Barducci, G. Bussi, M. Parrinello, Well-Tempered Metadynamics: A Smoothly Converging and Tunable Free-Energy Method. *Phys. Rev. Lett.* **100**, 020603 (2008).
  15. P. Raiteri, A. Laio, F. L. Gervasio, C. Micheletti, M. Parrinello, Efficient Reconstruction of Complex Free Energy Landscapes by Multiple Walkers Metadynamics. *J. Phys. Chem. B* **110**, 3533-3539 (2006).
  16. G. Bussi, F. L. Gervasio, A. Laio, M. Parrinello, Free-Energy Landscape for  $\beta$  Hairpin Folding from Combined Parallel Tempering and Metadynamics. *J. Am. Chem. Soc.* **128**, 13435-13441 (2006).
  17. S. Piana, A. Laio, A Bias-Exchange Approach to Protein Folding. *J. Phys. Chem. B* **111**, 4553-4559 (2007).
  18. Y. I. Yang, J. Zhang, X. Che, L. Yang, Y. Q. Gao, Efficient sampling over rough energy landscapes with high barriers: A combination of metadynamics with integrated tempering sampling. *J. Chem. Phys.* **144**, 094105 (2016).
  19. Y. I. Yang, H. Niu, M. Parrinello, Combining Metadynamics and Integrated Tempering Sampling. *J. Phys. Chem. Lett.* **9**, 6426-6430 (2018).
  20. O. Valsson, P. Tiwary, M. Parrinello, Enhancing Important Fluctuations: Rare Events and Metadynamics from a Conceptual Viewpoint. *Annu. Rev. Phys. Chem.* **67**, 159-184 (2016).
  21. G. Bussi, A. Laio, Using metadynamics to explore complex free-energy landscapes. *Nat. Rev. Phys.* **2**, 200-212 (2020).
  22. M. Bonomi, D. Branduardi, G. Bussi, C. Camilloni, D. Provasi *et al.*, PLUMED: A portable plug-in for free-energy calculations with molecular dynamics. *Comput. Phys. Commun.* **180**, 1961-1972 (2009).
  23. G. Fiorin, M. L. Klein, J. Hénin, Using collective variables to drive molecular dynamics simulations. *Mol. Phys.* **111**, 3345-3362 (2013).



24. M. Bonomi, A. Barducci, M. Parrinello, Reconstructing the equilibrium Boltzmann distribution from well-tempered metadynamics. *J. Comput. Chem.* **30**, 1615-1621 (2009).
25. P. Tiwary, M. Parrinello, A Time-Independent Free Energy Estimator for Metadynamics. *J. Phys. Chem. B* **119**, 736-742 (2015).
26. Y.-P. Huang, Y. Xia, L. Yang, J. Wei, Y. I. Yang *et al.*, SPONGE: A GPU-Accelerated Molecular Dynamics Package with Enhanced Sampling and AI-Driven Algorithms. *Chin. J. Chem.* **40**, 160-168 (2021).
27. J. Zhang, D. Chen, Y. Xia, Y.-P. Huang, X. Lin *et al.*, Artificial Intelligence Enhanced Molecular Simulations. *J. Chem. Theory Comput.* **19**, 4338-4350 (2023).
28. A. Hazel, C. Chipot, J. C. Gumbart, Thermodynamics of Deca-alanine Folding in Water. *J. Chem. Theory Comput.* **10**, 2836-2844 (2014).
29. J.-W. Chu, B. L. Trout, B. R. Brooks, A super-linear minimisation scheme for the nudged elastic band method. *J. Chem. Phys.* **119**, 12708-12717 (2003).
30. C. Bergonzo, A. J. Campbell, R. C. Walker, C. Simmerling, A partial nudged elastic band implementation for use with large or explicitly solvated systems. *Int. J. Quantum Chem.* **109**, 3781-3790 (2009).
31. D. Mandelli, M. Parrinello, A modified nudged elastic band algorithm with adaptive spring lengths. *J. Chem. Phys.* **155** (2021).
32. W. E, W. Ren, E. Vanden-Eijnden, String method for the study of rare events. *Phys. Rev. B* **66**, 052301 (2002).
33. B. Peters, A. Heyden, A. T. Bell, A. Chakraborty, A growing string method for determining transition states: Comparison to the nudged elastic band and string methods. *J. Chem. Phys.* **120**, 7877-7886 (2004).
34. L. Maragliano, A. Fischer, E. Vanden-Eijnden, G. Ciccotti, String method in collective variables: Minimum free energy paths and isocommittor surfaces. *J. Chem. Phys.* **125** (2006).
35. D. Branduardi, J. D. Faraldo-Gómez, String Method for Calculation of Minimum Free-Energy Paths in Cartesian Space in Freely Tumbling Systems. *J. Chem. Theory Comput.* **9**, 4140-4154 (2013).
36. L. Zhu, F. K. Sheong, S. Cao, S. Liu, I. C. Unarta *et al.*, TAPS: A traveling-salesman based automated path searching method for functional conformational changes of biological macromolecules. *J. Chem. Phys.* **150** (2019).
37. P. Maragakis, A. van der Vaart, M. Karplus, Gaussian-Mixture Umbrella Sampling. *J. Phys. Chem. B* **113**, 4664-4673 (2009).
38. G. A. Tribello, M. Ceriotti, M. Parrinello, A self-learning algorithm for biased molecular dynamics. *Proc. Nat. Acad. Sci. U.S.A.* **107**, 17509-17514 (2010).
39. J. Debnath, M. Parrinello, Gaussian Mixture-Based Enhanced Sampling for Statics and Dynamics. *J. Phys. Chem. Lett.* **11**, 5076-5080 (2020).
40. N. M. Mascarenhas, J. Kästner, How maltose influences structural changes to bind to maltose-binding protein: Results from umbrella sampling simulation. *Proteins* **81**, 185-198 (2013).
41. H. Sun, S. Tian, S. Zhou, Y. Li, D. Li *et al.*, Revealing the favorable dissociation pathway of type II kinase inhibitors via enhanced sampling simulations and two-end-state calculations. *Sci. Rep.* **5**, 8457 (2015).
42. W. You, Z. Tang, C.-e. A. Chang, Potential Mean Force from Umbrella Sampling Simulations: What Can We Learn and What Is Missed? *J. Chem. Theory Comput.* **15**, 2433-

- 2443 (2019).
43. H. Chen, D. Ogden, S. Pant, W. Cai, E. Tajkhorshid *et al.*, A Companion Guide to the String Method with Swarms of Trajectories: Characterisation, Performance, and Pitfalls. *J. Chem. Theory Comput.* **18**, 1406-1422 (2022).
  44. A. Hulm, C. Ochsenfeld, Improved Sampling of Adaptive Path Collective Variables by Stabilised Extended-System Dynamics. *J. Chem. Theory Comput.* **19**, 9202-9210 (2023).
  45. D. Branduardi, F. L. Gervasio, M. Parrinello, From A to B in free energy space. *J. Chem. Phys.* **126** (2007).
  46. G. Díaz Leines, B. Ensing, Path Finding on High-Dimensional Free Energy Landscapes. *Phys. Rev. Lett.* **109**, 020601 (2012).
  47. J. Zhang, Y.-K. Lei, Z. Zhang, J. Chang, M. Li *et al.*, A Perspective on Deep Learning for Molecular Modeling and Simulations. *J. Phys. Chem. A* **124**, 6745-6763 (2020).
  48. X. Liu, J. Zhang, Z. Hou, Y. I. Yang, Y. Q. Gao, From predicting to decision making: Reinforcement learning in biomedicine. *Wiley Interdiscip. Rev. Comput. Mol. Sci.* **14**, e1723 (2024).
  49. J. Zhang, Y. I. Yang, F. Noé, Targeted Adversarial Learning Optimized Sampling. *J. Phys. Chem. Lett.* **10**, 5791-5797 (2019).